Materials Today Bio 16 (2022) 100437

Contents lists available at ScienceDirect

Materials Today Bio

journal homepage: www.journals.elsevier.com/materials-today-bio

Self-snapping hydrogel-based electroactive microchannels as nerve guidance conduits

Jordi Amagat [a,b], Yingchun Su [a,c], Frederik Højberg Svejsø [a], Alice Le Friec [a], Steffan Møller Sønderskov [d], Mingdong Dong [d], Ying Fang [e,f], Menglin Chen [a,d,*]

[a] Department of Biological and Chemical Engineering, Aarhus University, Denmark
[b] Sino-Danish College (SDC), University of Chinese Academy of Sciences, Beijing, 101400, China
[c] School of Electrical Engineering and Computer Science, KTH Royal Institute of Technology, Electrum 229, 16440, Kista, Sweden
[d] Interdisciplinary Nanoscience Center, INANO, Aarhus University, Denmark
[e] CAS Center for Excellence in Nanoscience, National Center for Nanoscience and Technology, Beijing, 100190, China
[f] CAS Center for Excellence in Brain Science and Intelligence Technology, Institute of Neuroscience, Chinese Academy of Sciences, Shanghai 200031, China

ARTICLE INFO

Keywords:
Hydrogel
Anisotropic
Graphitic carbon nitride
Graphene oxide
Snapping
Nerve guidance conduit

ABSTRACT

Peripheral nerve regeneration with large defects needs innovative design of nerve guidance conduits (NGCs) which possess anisotropic guidance, electrical induction and right mechanical properties in one. Herein, we present, for the first time, facile fabrication and efficient neural differentiation guidance of anisotropic, conductive, self-snapping, hydrogel-based NGCs. The hydrogels were fabricated via crosslinking of graphitic carbon nitride (g-C_3N_4) upon exposure with blue light, incorporated with graphene oxide (GO). Incorporation of GO and *in situ* reduction greatly enhanced surface charges, while decayed light penetration endowed the hydrogel with an intriguing self-snapping feature by the virtue of a crosslinking gradient. The hydrogels were in the optimal mechanical stiffness range for peripheral nerve regeneration and supported normal viability and proliferation of neural cells. The PC12 cells differentiated on the electroactive g-C_3N_4 H/rGO3 (3 mg/mL GO loading) hydrogel presented 47% longer neurite length than that of the pristine g-C_3N_4 H hydrogel. Furthermore, the NGC with aligned microchannels was successfully fabricated using sacrificial melt electrowriting (MEW) moulding, the anisotropic microchannels of the 10 μm width showed optimal neurite guidance. Such anisotropic, electroactive, self-snapping NGCs may possess great potential for repairing peripheral nerve injuries.

1. Introduction

Peripheral nerve injuries (PNI) are a frequent complication of accidents and illnesses [1,2]. Depending on the site of the injury and the physiological characteristics of each individual, the human body has capacity to self-regenerate at approximately 3 mm/day [3]. However, when the axon cut leaves larger gaps (>20 mm), the body fails to self-repair, followed with the formation of scar tissue and induction of cellular apoptosis [4]. Some symptoms may appear, including loss of functionality, sensibility, or loss of motor functions. To avoid this, surgery will be necessary [5], where autografts or autogenous nerve grafts are the "gold standard" in surgical operation. Usually, the sural nerve is used as autografts together with viable Schwann cells. The self-sacrifice donor site will face some problems, such as sensory loss and neuroma formation. Allografts are readily available and will avoid donor site morbidity, however, they can produce highly immunogenic responses [6]. Alternative strategies are thus required, such as biomaterial-based therapies, which, with adequate development, have the potential to solve the availability problem, reduce immunogenic responses and provide biochemical and biophysical signals to guide nerve regeneration.

Hydrogels are three-dimensional (3D) crosslinked hydrophilic polymer networks and have gained huge interest in neural tissue engineering due to their structural and soft mechanical resemblance to the natural components of the extracellular matrix (ECM) [7,8]. Among many physical/chemical crosslinking systems, photo-crosslinked hydrogels have drawn enormous attention in tissue engineering due to the efficiency and accuracy of using light. Gelatin-methacrylate (GelMA) hydrogels have been used for vascular cells, fibroblasts and neural cells transplantation by crosslinking under UV light exposure [9–11]. Other hydrogels, such as PVA and chitosan-based hydrogel have also been

* Corresponding author. Aarhus University, Universitetsbyen 36, 8000, Aarhus C, Denmark.
E-mail address: menglin@bce.au.dk (M. Chen).

https://doi.org/10.1016/j.mtbio.2022.100437
Received 25 July 2022; Received in revised form 20 September 2022; Accepted 22 September 2022
Available online 22 September 2022

reported crosslinkable with UV light [12–14]. Emergingly, graphitic carbon nitride (g-C_3N_4), a graphene derived semiconductor with high visible light adsorption and excellent photocatalytic activity [15], has been shown to act as a highly efficient photo-initiator and hydrogel reinforcer in *N,N*-dimethylacrylamide (DMA)-based networks [16]. Importantly, such g-C_3N_4 hydrogels could be crosslinked under visible-light irradiation, avoiding UV-derived cell toxicity. However, hydrogels generally are isotropic and lack topographical cell guidance. Several efforts have been made to generate anisotropic hydrogels, such as sacrificial moulding or 4D printing to dynamically control hydrogel properties [17].

Melt electro-writing (MEW) is an emerging technique which consists of precisely controlled melt polymer deposition under a high voltage electric field. Incorporating MEW structures in hydrogels have been reported to enhance the mechanical properties [18–20]. Meanwhile, MEW scaffolds have already been researched as topological guiding components for neural cells [21], muscle cells [22] and as a capture-and-culture device of circulating tumour cells [23].

Electroactive materials have been used in neural tissue to interface with neurons and promote tissue regeneration. In order to introduce electrical properties, *Zhou* et al. [24] fabricated a soft conductive hydrogel based on tannic acid and conductive polymer, polypyrrole, for spinal cord repair. The conductive hydrogel activated neural stem cells and induced significant recovery of locomotor function both *in vitro* and *in vivo*. Recently, graphene related materials such as graphene oxide (GO) have been used to increase conductive properties of biomaterials. For instance, Guo et al. functionalized reduced graphene oxide (rGO) into an acellular matrix, which promoted the differentiation of mesenchymal stem cells (MSCs) to neuronal cells [25]. In another study, an ionic hydrogel with high conductivity and suitable mechanical properties was generated [26].

Herein, we present, for the first time, the facile fabrication and efficient neural differentiation guidance of anisotropic, electroactive, snapping g-C_3N_4/rGO hydrogels, with great potential as nerve guidance conduits (NGCs) (Scheme 1). Incorporating rGO into g-C_3N_4 hydrogels not only introduced electroactivity, but also induced intriguing self-snapping property that could potentially ease the implantation procedure. MEW polycaprolactone (PCL) patterns were used as a sacrificial template to introduce the anisotropic microchannels in the NGCs. The morphology, swelling, surface charges and mechanical properties of the hydrogels were characterized by SEM, swelling analysis, quantitative surface conductivity microscopy (QSCM), and compressive analysis, respectively. The biocompatibility and neural differentiation induction of the hydrogels were investigated using a neural model cell line, PC12 cells [27]. The electrical induction of PC12 differentiation on the conductive g-C_3N_4 H/rGO hydrogel was compared with that of g-C_3N_4 H. Snapping of the g-C_3N_4 H/GO-NGC was characterized and the size of the anisotropic channels for neural guidance was optimized.

2. Materials and methods

2.1. Fabrication of g-C_3N_4 and GO

g-C_3N_4 nanosheets were produced as reported before via synthesis from urea [28]. Briefly, 10 g of Urea (Merck) were introduced in a crucible and were treated at 550 °C for 4 h. Afterwards, the product was grounded to powder and stored into a dry dark place. GO nanosheets were synthesized via Modified Hummer's method, as prepared before, via oxidation and physical exfoliation of graphite powder [21].

2.2. g-C_3N_4 hydrogel fabrication

g-C_3N_4 hydrogels were fabricated following a protocol from *Kumru* and co-workers [16]. Shortly, 30 mg of g-C_3N_4 were added to 4.6 mL of dH_2O and ultrasonicated in ice bath for 5 min using an amplitude of 60% and 1 s intervals (SonoPlus HD 2200.2, MS73 probe). Ultrasonication treatment was repeated 3 times to form homogeneous dispersion. After the sonication, 4 mg of N,N′-methylenebis(acrylamide) (MBA, Merck) were added to the mixture. 400 μL of *N,N*-dimethylacrylamide (DMA, Merck) were added after passing through an inhibitor removal column (Merck). The solution was loaded into syringes (VWR) for a further injection into a 25 × 60 × 1.1 mm^3 glass mould and crosslinked under 450 nm blue light for 4 h. The blue light was a custom-made LED matrix consisting of 192 LED chips (50 mW/cm^2) with a cooling fan to avoid

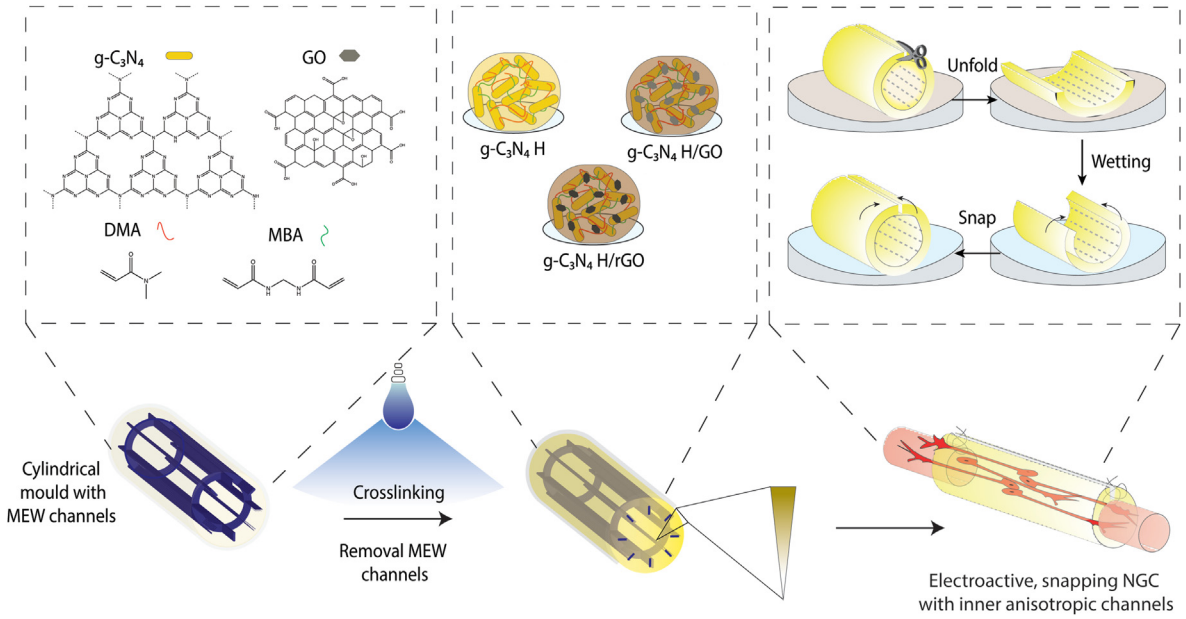

Scheme 1. Illustration of the anisotropic, conductive, snapping NGC. g-C_3N_4, DMA and MBA can be used to generate g-C_3N_4 H upon crosslinking under blue light. Addition of GO will produce g-C_3N_4 H/GO, which after mild AA reduction *in situ* will change to g-C_3N_4 H/rGO. Incorporation of GO hinders light penetration, and crosslinking of inner areas, hereby generating a radial gradient of crosslinking. Upon wetting, NGC would recover their cylindrical original shape. Sacrificial MEW fiberous template can be introduced before crosslinking, which will generate anisotropic inner channels. The combination of the anisotropic channels, rGO, and snapping properties could be used to generate an anisotropic, conductive, snapping NGC.

overheating and the distance from source to mould was fixed to 3 cm. After crosslinking, hydrogels were taken out of the mould and dialyzed against dH_2O for two days with changing the water twice. After 2 days, hydrogels were cut using a ∅6 mm biopsy puncher (Acuderm). The hydrogels were freeze-dried and stored for further use.

2.3. GO and rGO hydrogel fabrication

GO hydrogels were fabricated using a similar process as non-loaded g-C_3N_4 hydrogels. Briefly, different amounts of GO were added to the hydrogel mixture before the ultrasonication step (0, 0.1, 1 and 3 mg/mL GO). The rest of the process was kept unaltered.

To further reduce GO loaded hydrogels to rGO, ∅6 mm hydrogels were immersed into a 10 mg/mL ascorbic acid solution for 2 or 4 days at 37 °C with mild shaking. After two or four days, the hydrogels were removed and washed with dH_2O.

2.4. g-C_3N_4 hydrogel micro-channels

To create anisotropic patterned g-C_3N_4 hydrogel structure, melt electro-writing (MEW) scaffolds were used as sacrificial templates. Shortly, PCL (45 kDa, Merck) was loaded into a 24G stainless steel syringe and heated up to 80 °C. Sacrificial MEW fibers in parallel (spacing 200 μm) were printed on top of ITO conductive glass slides (75 × 25 mm, Diamond Coatings), which was connected to a grounded collector controlled by UCCNC software (Spraybase).

In order to print small fibers (~10 μm in diameter), printing speed was set to 1000 mm/min, air pressure was set to 0.15 bar, distance tip to collector was set to 4 mm, and applied voltage was set to 3.5 kV. To print medium fibers (~20 μm), 300 mm/min printing speed, 0.55 bar air pressure, 1 mm distance and 2 kV voltage were set. Finally, the settings to print thick fibers (~70 μm) were 50 mm/min, 0.55 bar, 1 mm and 2 kV. To keep the height of the scaffolds to be constant, 10 layers were printed for the smaller fibers, 4 layers for the medium fibers and 2 layers for the thick fibers.

G-codes controlling the UCCNC software to generate the microfibrous patterns with 200 μm spacing are included in the Supplementary Table S1. After printing the scaffolds onto the transparent conductive glass, the conductive slides were incorporated into the mould, and g-C_3N_4 hydrogel solution was added for crosslinking. After crosslinking and dialysis, the NGCs were soaked in DCM for 12 h in mild shaking to remove the MEW sacrificial fibers and generate the channels (Fig. S1).

2.5. Snapping g-C_3N_4 NGCs with MEW channels

Snapping g-C_3N_4 tube was prepared as following: 30 mg of g-C_3N_4 and 1 mg/mL GO were mixed into 4.6 mL of MilliQ H_2O and ultrasonicated in ice bath. The ultrasonication condition and preparation process was the same as that in the section of g-C_3N_4 hydrogel fabrication. 4 mg of MBA and 400 μL of DMA were added. Afterwards, the mixed solution was loaded into 1 mL syringes (VWR, inner diameter 4.71 mm). After crosslinking for 4.5 h under 450 nm blue light, the hydrogel was dialysed against diH2O for 2 days. The as-prepared hydrogel tubes were freeze dried and stored for further characterization. For NGCs with MEW sacrificial channels, the MEW grids (200 μm × 1000 μm, G-code in Table S2) were inserted into the solution in the syringe before crosslinking. After crosslinking and dialysis, the NGCs were soaked in DCM for 12 h to remove the MEW sacrificial fibers and generate the inner channels.

2.6. Scanning electron microscopy (SEM)

The morphology of scaffold was characterized by scanning electron microscopy (SEM, TM3030Plus, Tabletop microscope, HITACHI). The acceleration voltage was set to 15 kV. Briefly, scaffolds were punched out using a 4 mm biopsy puncher (Acuderm) and placed into a double-sided conductive carbon tape on top of a specimen stage.

2.7. Swelling assay

In order to investigate the swelling capacity of the g-C_3N_4 hydrogels, 6 replicates were freeze-dried for 48 h and immersed in excess PBS (pH 7.4, ThermoFisher). Briefly, for each measurement, the hydrogels were taken out from the bath, the excess water was dried using a tissue paper and they were weighted using a scale. The swelling ratio (Q) was calculated using the following formula:

$$Q = \frac{Weight_{swollen} - Weight_{dry}}{Weight_{dry}}$$

The measurements were done at 22.5 °C and 30% of humidity.

2.8. Mechanical compression analysis

Mechanical axial-compression testing was measured by a Bose ElectroForce 3200 Series II Test Instrument with a compression rate of 0.025 mm/s. The compression tests were performed under room temperature. The hydrogel samples (diameter of 3 mm and height of 1.2 mm) were placed between the testing plates. The Young's modulus was calculated according to the following formula:

$$\text{Young}'\text{s modulus} = \frac{\text{Stress}}{\text{Strain}} = \frac{F/A}{(L - L_0)/L_0}$$

where F is the applied compressive force, A is the cross-section area perpendicular to the direction of force, L-L_0 is the length change, and L_0 is the initial length.

2.9. Surface charge measurements

Surface charge density (SCD) measurements were performed using a scanning ion conductance microscope (SICM) setup on an XE-Bio system (Park Systems, Suwon, South Korea) using Ag/AgCl electrodes. The imaging buffer consisted of 10 mM HEPES (pH 7.0) and 150 mM KCl. A single borosilicate glass nanopipette was used for all measurements. SCD sensitive current-distance curves were obtained at an approach and withdraw speed of 200 nm s^{-1} at potentials of ±0.5 V. For each sample, current curves obtained at ±0.5 V were first normalized with respect to the bulk current. Following this, the two curves were subtracted from each other, (+)100 mV-(−)100 mV yielding ΔI_N. Multiple curves were obtained at various locations for verifying the curve tendencies. The curves shown are representative of the SCD properties.

2.10. Atomic force microscopy (AFM)

AFM imaging was performed in air using PeakForce Tapping on a MultiMode 8 AFM (Bruker, USA) using SNL-10 (Bruker, USA) probes. Scans were acquired at a scan-rate of 1 Hz, 256 lines and an image size of 10 μm. The final AFM images were flattened using SPIP software (Image Metrology ApS, Lyngby, Denmark).

2.11. PC12 cells culture

PC12 cells are derived from a rat adrenal pheochromocytoma. Due to their differentiation into neuron-like cells, they have been widely used as a model for peripheral nerve studies. PC12 cells were incubated at 37 °C in humidified atmosphere of 5% CO_2 (Panasonic). Media was replaced every second day.

Hydrogels were seeded with dynamic seeding. 20 μL of PC12 cells solution were seeded on freeze-dried collagen-coated hydrogels at a concentration of 30,000 cells per scaffold in a 96-well plate (Starsted).

After seeding, cells were moved into the shaking incubator (100 rpm) immediately for 30 min. Then 180 μL of media were added. For porous scaffolds, dynamic seeding has been observed to increase significantly the cell seeding efficiency [29–31].

2.12. Proliferation

PC12 cells were grown in collagen IV (Merck) coated flasks and maintained in DMEM/F:12 (Gibco), supplemented with 15% Horse-Serum (HS, Gibco), 2.5% Fetal Bovine Serum (FBS, Gibco), 1% Penicillin/Streptavidin (P/S, Gibco) and 0.5% HEPES buffer (Merck).

2.13. Differentiation

For differentiation studies, growth media was replaced by neuronal differentiation media: DMEM/F:12, supplemented with 0.5% HS, 0.5% FBS, 1% P/S and 50 ng/mL of 2.5 S nerve growth factor (NGF, ThermoFisher).

2.14. Proliferation assay

Proliferation studies were performed using a CCK-8 commercial kit (Dojindo). Assay was performed following the manufacturer's instructions: cell culture media was removed and 100 μL of CCK-8 solution were added (1:10 dilution with growth media). Samples were incubated for 3 h; the solutions were transferred to a new plate and the absorbance was measured at 450 nm using a plate reader (Viktor X5, Perkin Elmer). Proliferation index was calculated using the following formula [21]:

$$PI_x = \frac{Ab_x}{Ab_1}$$

where PI_x is the proliferation index, and Ab_x is the absorbance value at 450 nm from the CCK-8 assay measured at day x (x = 1, 3, 5 and 7).

2.15. Cytotoxicity assay

Cytotoxicity studies were performed according to manufacturer's instructions (LDH cytotoxicity kit, Roche). Briefly, 100 μL of cell culture media were centrifuged for 5 min at 1700 rpm at 4 °C. 50 μL of the supernatant were mixed with 50 μL of the reaction mix (Catalyst and dye, in a 1:45 ratio) in a 96-well plate. After 30 min incubation at room temperature, absorbance was measured at 490 nm. High toxicity control was performed with the supplementary addition of 1% Triton X-100 in cell culture media, and cells grown on TCP as the low toxicity control. Cytotoxicity was calculated using the following formula:

$$Cyotoxicity = \frac{Exp.\ value - low\ control}{high\ control - low\ control}\ x\ 100$$

2.16. Live-dead assay

Live-dead assay was used to assay cell viability at day 7 in the middle of the experiment. Cells were washed once with warm DMEM medium without Phenol Red (Gibco) once and stained for 15 min with Calcein AM (1–1000 dilution) and Propidium Iodide (PI, 1 to 500 dilution) in DMEM media without phenol red. Cells were observed under a fluorescent microscope.

2.17. Immunostaining and fluorescence imaging

PC12 cells were stained as reported previously [21]: 4% (v/v%) formaldehyde (Merck) and 0.2% Triton-X in PBS were prepared for cell fixation and membrane permeabilization, respectively. After blocking with 1% BSA (Merck) solution in PBS, PC12 cells were stained with a rabbit anti-βIII tubulin antibody (TUJ1, Abcam, 1:1000) as a primary antibody, and a donkey anti-rabbit-AlexaFluor-594 antibody (Abcam, 1:1000) as a secondary antibody. Fluorescence images were taken by a EVOS FL Auto Cell Imaging system (ThermoFisher), equipped with DAPI, GFP and TxRed filter cubes (ThermoFisher) or Zeiss LSM 700 laser confocal microscope (Carl Zeiss Micro-Imaging GmbH).

Neurite outgrowth was quantified using ImageJ plugin NeuronJ as described previously [21]. Briefly, groups were blinded, images were calibrated, and the channels were split. After loading the images to NeuronJ, neurites were quantified following these rules: Only neurites larger than the cell body were counted, in case of neurite branches, only the longest neurite was counted. At least 100 neurites were counted for each condition and each group.

2.18. Statistics

Statistics were performed with GraphPad Prism. Data is shown in replicates. Results are expressed as mean and standard deviations as error bars.

Statistical analysis was performed in the different groups using t-tests, One or Two-way ANOVA packages in Prism 9 (GraphPad). Statistical significance was considered at $p < 0.0332$.

3. Results and discussion

3.1. Fabrication and characterization of g-C_3N_4/GO-based hydrogels

The as-prepared fresh g-C_3N_4 hydrogels (g-C_3N_4 H) had a pale-white color, soft appearance (Fig. 1A, A′). To improve charge transfer [28,32], g-C_3N_4 hydrogels were loaded with GO (Fig. 1B–D, B′-D′). 0.1, 1 and 3 mg/mL of GO were directly loaded into the hydrogels (marked as g-C_3N_4 H/GO0.1, g-C_3N_4 H/GO1, g-C_3N_4 H/GO3, respectively) and gelation remained stable. Higher concentration of GO (5 mg/mL) lead to poor crosslinking and incomplete gelation. SEM images showed that all hydrogels had an interconnected network of micropores (Fig. 1), which could be beneficial for cell infiltration or potential drug delivery [27].

g-C_3N_4 H hydrogels had smooth pores (Fig. 1A), which became rough and irregular with the loading of GO, especially obvious with the highest concentration of GO, g-C_3N_4 H/GO3 (Fig. 1B–D).

GO in its reduced form, reduced graphene oxide (rGO) possesses numerous advantages with enhanced conductivity, cell attachment, increased nerve cells growth and neurite extension [33,34]. Mild reduction of GO using AA caused darkened color, while it didn't affect internal structure or pore morphology (Fig. 1B'-D′).

Swelling of g-C_3N_4 H, g-C_3N_4 H/GO and g-C_3N_4 H/rGO hydrogels was also analysed (Fig. 1E). g-C_3N_4 H were able to increase their initial dry weight by 25.4-fold when exposed to a PBS solution. When hydrogels were loaded with 0.1, 1 and 3 mg/mL GO, the swelling ratio was reduced to 22, 17 and 18-fold, respectively, which shows that the introduction of GO into the g-C_3N_4/H network restricted the swelling performance [35]. The reduction of GO to rGO inside the network of the hydrogels didn't induce significant changes in swelling. The reduction time was also considered, and there were no differences between the samples reduced for 2 days and 4 days.

For characterization of the hydrogel surface charge density (SCD), a nanopipette based method termed quantitative surface conductivity microscopy (QSCM) was used [36]. QSCM has been applied for high-resolution surface charge studies of biological and inorganic surfaces [37,38]. Here, current moving through a nanopipette is dependent on the sample SCD when in its vicinity, and thus can be utilized as a nanoscale SCD sensor [39]. Fig. 1F examines the g-C_3N_4 H and g-C_3N_4 H/rGO hydrogels SCD by showing ΔNormalized current curves obtained at potentials of ±0.5 V, while the raw current-distance curves can be found at Supplementary Fig. S2. Here, in all cases, an increase in

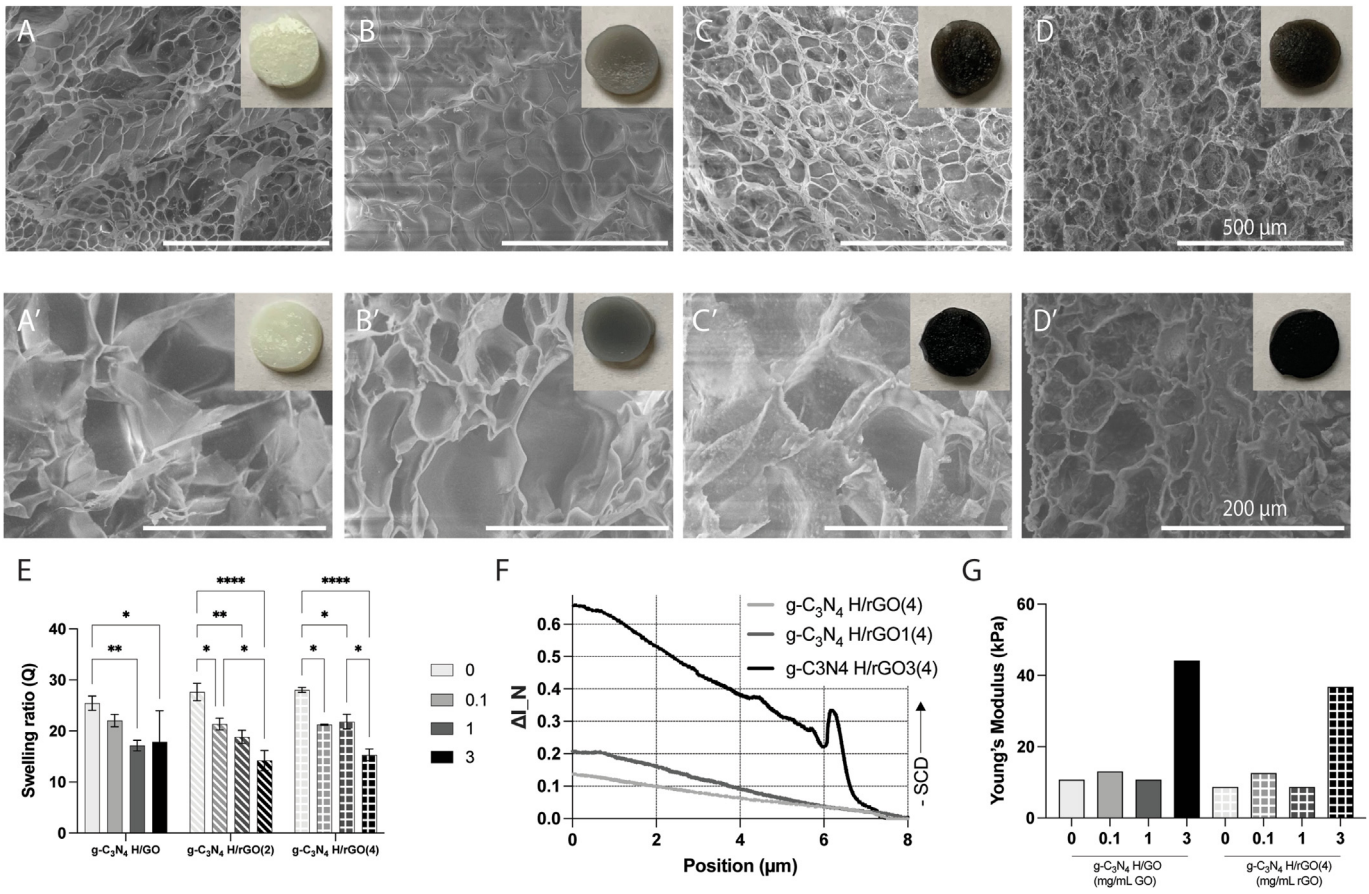

Fig. 1. Characterization of g-C_3N_4 hydrogels. Cross-section SEM images and visible pictures (inset) of g-C_3N_4 H (A) and g-C_3N_4 H/GO (B-D, 0.1, 1 and 3, respectively). Scale bars: 500 μm. Hydrogels were mild reduced for 4 days (A′-D′, equal concentrations as A-D). Scale bars: 200 μm. Swelling analysis (E) of g-C_3N_4 H with different GO loadings and reduction times (g-C_3N_4 H/GO: No reduction. g-C_3N_4 H/rGO(2): 2-day reduction and g-C_3N_4 H/rGO(4):4-day reduction). QSCM analysis (F) of g-C_3N_4 H/rGO(4) hydrogels. Δ Normalized current curves for hydrogels with different concentrations of GO. Mechanical characterization (G) of g-C_3N_4 H/GO and g-C_3N_4 H/rGO(4). Statistical data are denoted as *p < 0.0332, **p < 0.0021, ***p < 0.002 and ****p < 0.0001.

ΔNormalized current when the nanopipette approaches and indents the hydrogel was observed, which evidences that all hydrogel samples contain a negative SCD. Interestingly, it is also observed that as the rGO content increases, so does negative surface charge density.

Mechanical properties of the hydrogels were characterized via a compressive test. Hydrogels mimicking the mechanical properties of native brain tissue, have already been reported [24]. Young's Modulus of native brain tissue is around 5–13 kPa. Stiffness of the peripheral nerve tissue, on the other hand, ranges from 6 to 50 kPa, and increases with age [40,41]. After obtaining the stress-strain curves, the Young's Modulus of the linear compressive region was calculated (Fig. 1F). The Young's Modulus was approximately 10 kPa for unloaded hydrogels and GO-loaded hydrogels below 1 mg/mL GO. The Young's Modulus increased substantially when hydrogels were loaded with 3 mg/mL GO (g-C_3N_4 H/rGO3), at around 44 kPa. The Young's Modulus of the hydrogels after 4-day reduction was unaltered (Fig. 1G). All hydrogels analysed were in the optimal mechanical stifness range for peripheral nerve regeneration [40].

Derivatives of g-C_3N_4 hydrogels have been reported recently. For instance, Tong and co-authors [15] generated a 3D aerogel with g-C_3N_4 and GO, which could degrade methyl orange up to 92% within 4 h of light exposure (λ > 420 nm, 500 W). Similarly, other g-C_3N_4/GO-based PEGDMA hydrogels with high photocatalytic properties have been reported. Commonly, most of them include a highly porous structure which improves visible-light absorption and an electron transfer through an interconnected network [42].

3.2. Biocompatibility of g-C_3N_4/GO-based hydrogels for neural cells

Then, we investigate for the first time, whether the hydrogels could serve as a biocompatible and non-cytotoxic platform for 3D cell culture or tissue engineering, especially for neural cells. The biocompatibility of g-C_3N_4 H was evaluated *in vitro* by live/dead, cytotoxicity and proliferation assays. PC12 cells were grown on top of g-C_3N_4 H, and after 7 days of culture, cells were stained by live/dead assays (Fig. 2A). All types of hydrogels show a high percentage of live cells (Fig. 2A top row) and very low to none of dead cells (Fig. 2A lower row). In growth culture, PC12 cells showed irregular-round morphology and growth in clusters. 6–22% cytotoxicity was observed for all hydrogels analysed on the LDH assay (Fig. 2B). There is no significance among g-C_3N_4 H/GO and g-C_3N_4 H/rGO groups. This is in agreement of normal cell proliferation analysed with a cell counting kit (CCK-8), which measures metabolic activity of live cells (Fig. 2C).

Loading of GO into hydrogels have been reported to increase cellular adhesion. In addition, no GO nanoparticles were leaking from the hydrogels and no morphological changes were observed over 20 days of culture, which showed stability of the hydrogels (Fig. S3). Similar to the results reported in Fig. 2A, *Park* et al., reported loading of GO into GelMA hydrogels, which led to a more homogenous cell distribution compared to pristine GelMA, where cells grew in cluster-like shapes [34]. GO and nanomaterials have been reported to increase cellular attachment due to their affinity to interact with ECM proteins and to increase surface roughness.

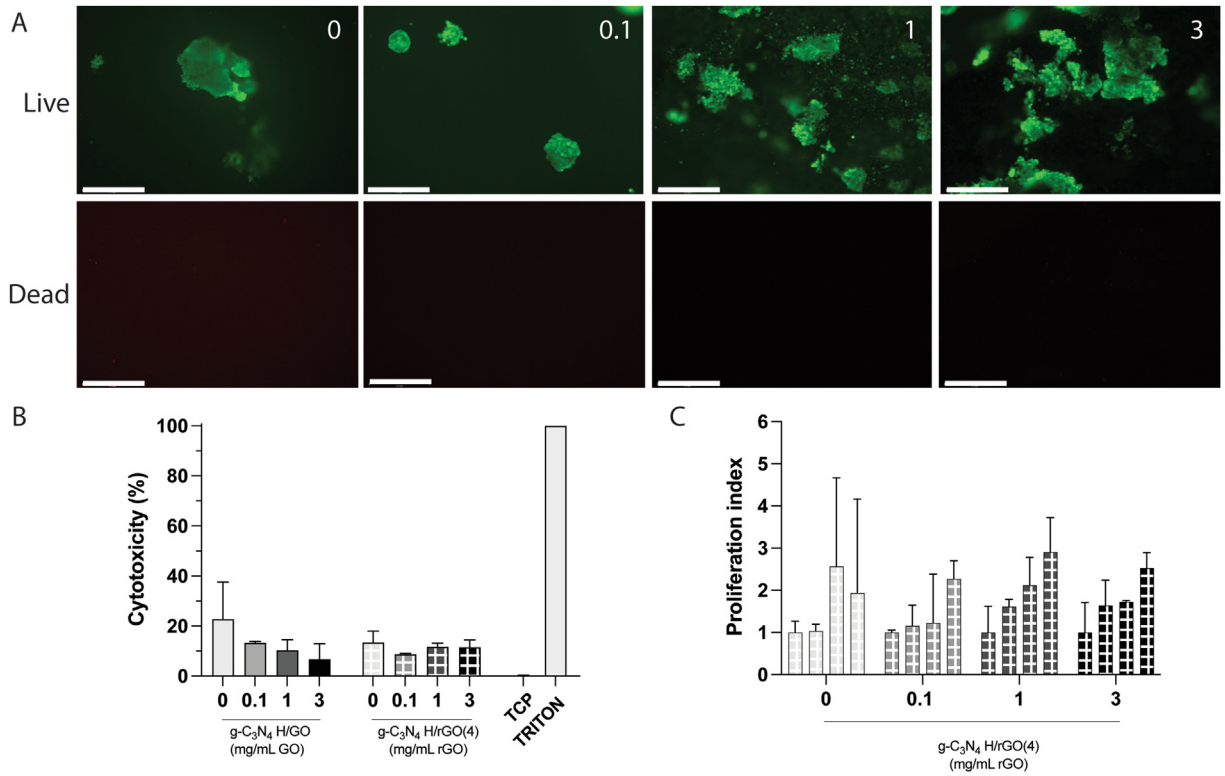

Fig. 2. Biocompatibility and cytotoxicity of g-C_3N_4 H and g-C_3N_4 H/GO over PC12 cells. (A)Live-dead analysis. Green: Live cells. Red: Dead cells. Scale bars: 275 μm. No dead cells are visible in the representative pictures. (B). Cytotoxicity LDH assay after 24 h of culture. (C). Proliferation assay CCK-8 over 1, 3, 5 and 7 days of culture on g-C_3N_4 H/rGO(4). (For interpretation of the references to colour in this figure legend, the reader is referred to the Web version of this article.)

3.3. g-C_3N_4/rGO hydrogel with enhanced conductivity significantly enhance neurite extension

In addition, carbon nanomaterials with enhanced conductivity have also been reported to increase neurons electrical signalling [43]. PC12 cells differentiated on top of g-C_3N_4 H had an average neurite length of 59.5 ± 31.2 μm. No significant differences in neurite length are observed when the g-C_3N_4 H are exposed to AA regardless of the exposure time (Fig. 3D. 51.9 ± 25.4 and 56.7 ± 29.8 μm, respectively, for 2- and 4-days reduction). When the hydrogels are loaded with 1 mg/mL GO, the average neurite length increases to 68.2 ± 36.8 μm. In addition, when g-C_3N_4 H/rGO1 were reduced for 2 and 4 days, neurite length significantly increased to 75.6 ± 45.4 and 92.7 ± 55.9 μm, respectively. Similarly, the same significant trend is shown when g-C_3N_4 H/GO3 were reduced. Non-reduced 3 mg/mL GO hydrogels had an average neurite length of 64.3 ± 39.2 μm (Fig. 3A), while the reduced hydrogels significantly increased the average neurite length to 72.7 ± 39.8 and 87.0 ± 48.3 μm, respectively, for 2 and 4 days of reduction (Fig. 3B and C).

Overall, our findings are consistent with previous reports. For example, *Liu* et al., developed a charged functionalized hydrogel as nerve conduits, where neurite length was enhanced by introducing conductive cues of rGO [33]. rGO functionalization has also been used for other electrically stimulable cells [44]. For instance, *Shin* et al., fabricated conductive hydrogels for cardiac tissue engineering. Cells grown on GelMA hydrogels loaded with rGO showed higher expression of cardiac markers and higher spontaneous beating compared to non-reduced GO hydrogels [35].

3.4. Construction of a snapping NGC with inner anisotropic channels

Further, we explored the assembly capabilities of g-C_3N_4 H/GO as NGCs. As mentioned in Fig. 1, crosslinking was hampered by high loading of GO. By virtue of decayed light penetration from GO (Fig. S4), a gradient of crosslinking is naturally produced when g-C_3N_4 H/GO1 solution was filled in a cylinder mould (Fig. 4A). Once crosslinked, hydrogels have a tubular shape, and can immediately snap upon immersion into aqueous solution, after manually opened up on a flat surface (Fig. 4B, C, D and Video S1). After analysing the macromolecular structure of the cross-section via SEM, a gradient in pore size was found, and the core was not crosslinked and thus left hollow. As seen in Fig. 4B, a high density smaller tighter pores are found in the outer region of the cylinder, whereas in the inside, a lower density larger pores are found. This difference in pore size and density would explain their shape memory to snap, which is consistent with the findings of *Fan* et al. [45]. In addition, topographical profiles were analysed. The inner, outer and cross-sectional AFM images show significantly different topographical profiles. Line-profiles are drawn to highlight this; for the cross-section sample, surface features of up to 10 nm can be seen, while the entire sample is relatively flat with a surface roughness (Sa) of 1.67 nm. For the outer part (high crosslinking zone) of the hydrogel, surface features are significantly larger extending up to several 100 nm and with a surface roughness of 27.86 nm. The features of the inner part (low crosslinking zone) are on the micro-meter scale with a surface roughness of 307.82 nm and numerous surface irregularities are observed (Fig. S5).

Finally, these snapping NGCs can be combined with the sacrificial MEW PCL moulding. In contrast to conventional electrospinning, where the fibers are deposited randomly into a collector, MEW has been previously used to generate computer-guided 3D scaffolds with controllable architecture. MEW patterns with 200 μm spacing could be internalized inside of the cylinders before crosslinking (Fig. 4E). After crosslinking with the hydrogel solution, these patterns could be dissolved by exposing the hydrogel to DCM. 3D MEW parallel fibrous scaffolds leave behind a series of inner channels inside the NGCs that could be used guide neurites extension and neuron regeneration (Fig. 4F, S6).

Self-folding NGCs have, so far, only been reported with thermo-responsive systems. For instance, *Zhang* et al. investigated the

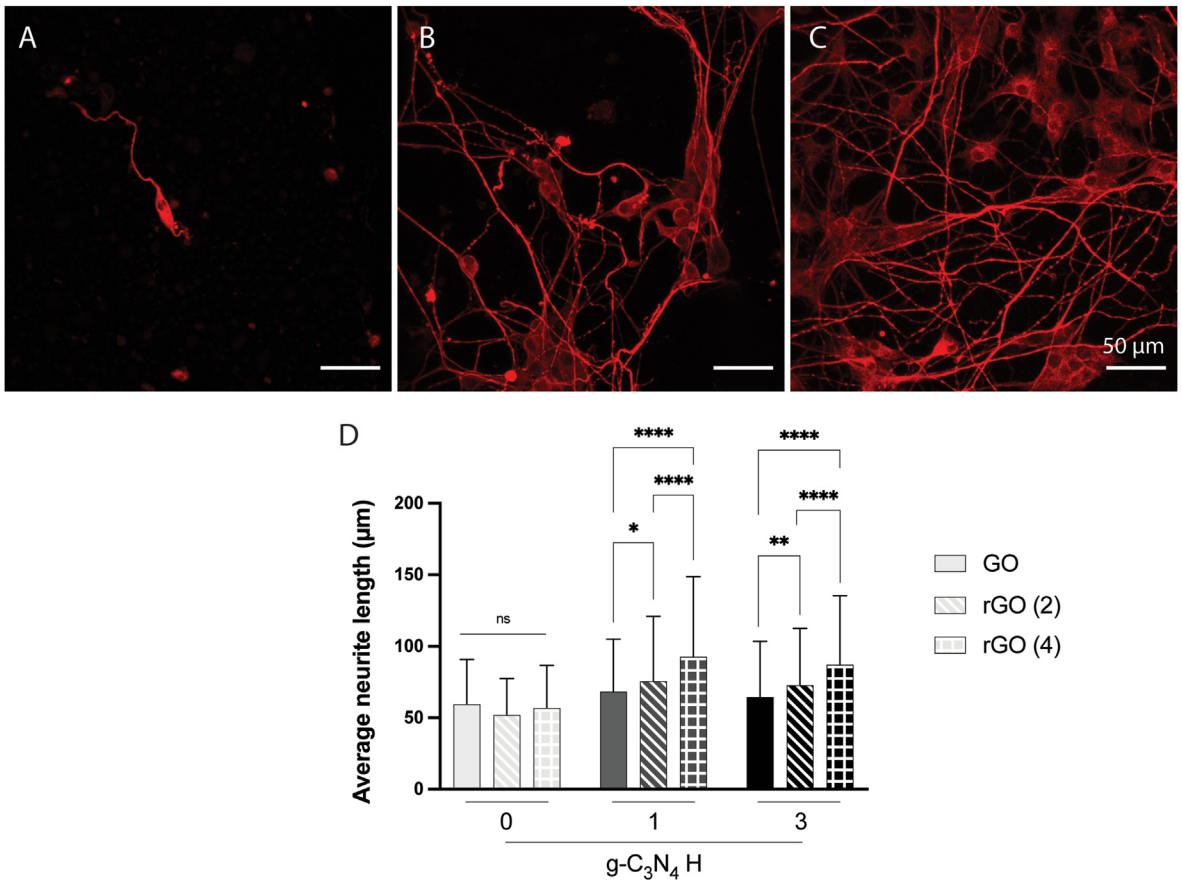

Fig. 3. PC12 cells differentiation on top of g-C_3N_4/H. Immunocytochemistry fluorescent images from PC12 cells cultured on top of g-C_3N_4 H/GO3 (A), g-C_3N_4 H/rGO3(2) (B) and g-C_3N_4/H/GO3(4) (C). Average neurite length of PC12 cells (D). Cells were stained with TUJ1 (red). Scale bars: 50 μm. Statistical data are denoted as *p < 0.0332, **p < 0.0021, ***p < 0.002 and ****p < 0.0001. (For interpretation of the references to colour in this figure legend, the reader is referred to the Web version of this article.)

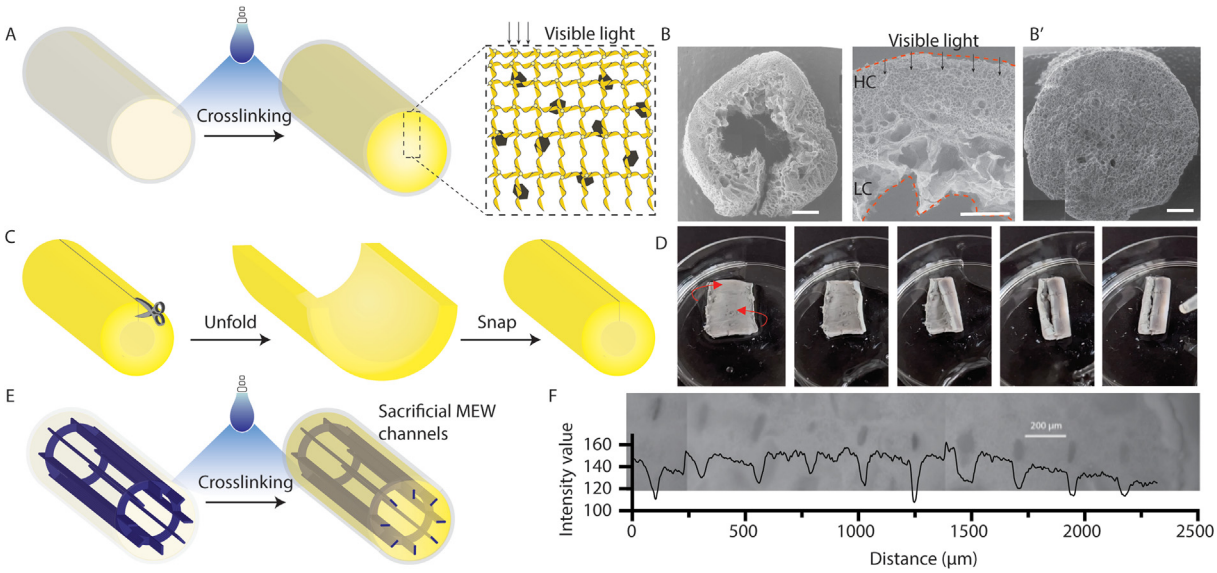

Fig. 4. Construction of a nerve guidance hydrogel conduit with snapping capabilities and introduction of inner anisotropic sacrificial channels. A. Scheme of the mechanism of producing differential crosslinking. B. Stitched SEM images of cross-section of g-C_3N_4 H/GO1 NGC, showing the tube structure. In detail, gradient of crosslinking of the snapping g-C_3N_4 H/GO1 NGC. High crosslinking (HC) zones are produced closer to the light source, while low crosslinking (LC) zones further from the light. B'. Cross-section SEM stitched image of a non-loaded g-C_3N_4 H. C. Mechanism of producing a snapping NGC. D. Visible images from a g-C_3N_4 H-NGC/GO snapping after being in contact with water; red arrows indicate snapping direction. E. Introduction of sacrificial melt electro written (MEW) scaffolds inside the NGC hydrogel generates anisotropic guiding channels. F. Grey-scale fluorescence image showing the anisotropic channels in g-C_3N_4 H generated by MEW scaffolds. Plot intensity grey value. Scale bars: B(left): 1 mm. B(right): 500 μm. B': 1 mm. (For interpretation of the references to colour in this figure legend, the reader is referred to the Web version of this article.)

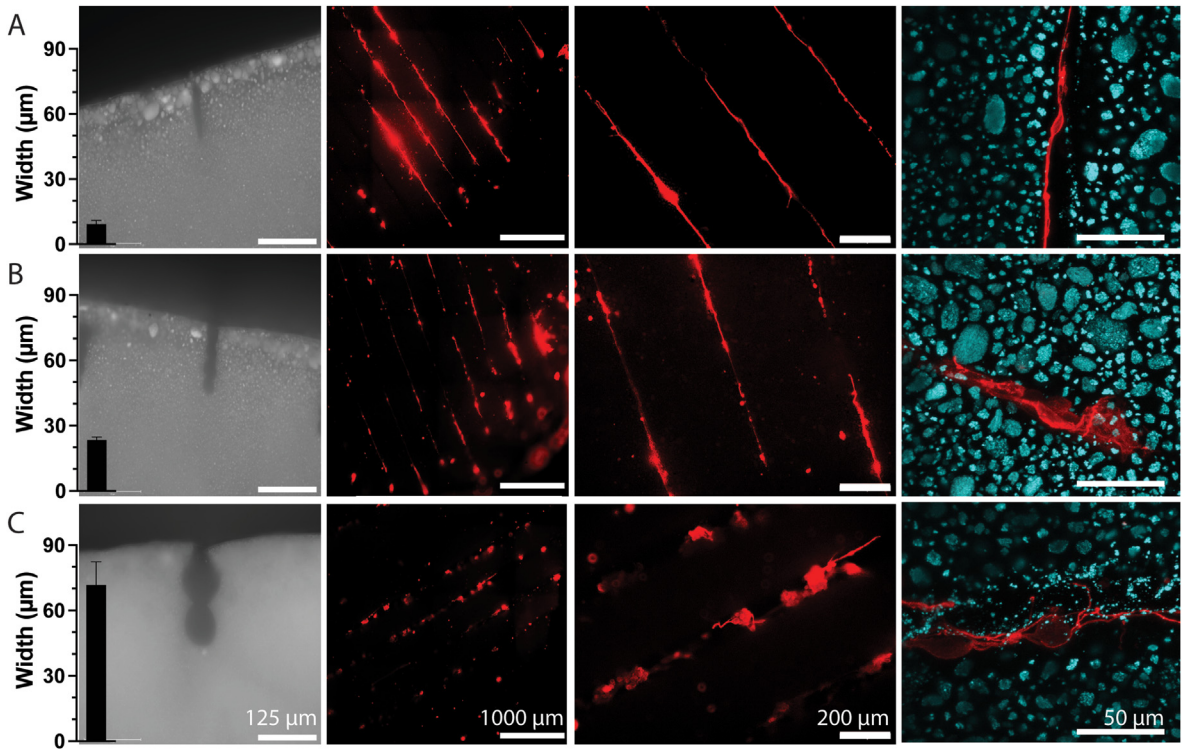

Fig. 5. Guidance effect from patterned g-C_3N_4 hydrogels. Microchannel width measured from the grey-scale fluorescent pictures and fluorescent microscopy images from PC12 cells differentiation on patterned anisotropic hydrogels with small, medium and large channel width (A, B and C, respectively.) Columns from left to right: Microchannel diameter, grey-scale fluorescent picture of the channel (scale bar 125 μm), stitched image of PC12 cells (scale bar 1000 μm), fluorescent image of channels with PC12 cells (scale bar 200 μm), and confocal fluorescent images of single cell (scale bar 25 μm). Cells were stained with TUJ1 (red). Autofluorescence of the g-C_3N_4 hydrogel is shown in confocal images (blue). (For interpretation of the references to colour in this figure legend, the reader is referred to the Web version of this article.)

combination of an electrospun poly(*N*-isopropylacrylamide) (PNIPAM) film with a MEW template to form as a bi-layer system. The thermoresponsive characteristics of the PNIPAM films induced the shrinkage mismatch between the bi-layer system in warm water, it self-folded into a tube [21]. In a similar manner, *Wang* and co-authors generated poly(-lactide-*co*-trimethylene carbonate) thermo-responsive nanofibers which self-folded when immersed in warm solutions [46]. Our new g-C_3N_4 H/GO snapping NGCs are straightforward to be fabricated and utilized without relying on temperature control.

3.5. Size optimization of anisotropic microchannels

As reported previously, neurite extension is strongly affected by anisotropic surface topography [21,47,48]. In order to further determine the optimal size of the channels introduced by sacrificial MEW PCL moulding (Fig. S1), anisotropic channels of around 120 μm depth with three different widths were generated and confirmed by fluorescent microscopy (Fig. 5). After complete hydration of the g-C_3N_4 H, microchannel diameters were 9.3 ± 1.6, 23.5 ± 1.2 and 71.7 ± 10.6 μm, respectively. PC12 cells differentiated for 10 days on top of anisotropic g-C_3N_4 H. As observed in Fig. 5A, PC12 neurites were only aligned along the thin microchannels (9.3 μm). As the channel width increased, the neurites alignment decreased (Fig. 5B and C). As shown in confocal microscopy images, the neurites appeared wavy and lost their alignment along the big channel.

Anisotropic hydrogels have been reported in the literature, mostly based on the strategy of supramolecular assembly [49,50]. Here, we report the fabrication of an anisotropic hydrogel with fully customizable surface topographies, via a sacrificial MEW mould. Sacrificial patterns have been widely used in tissue engineering, for both solid scaffolds and hydrogel materials. Some examples include cellulose hydrogel tubes, which were further degraded to produce tubular cell sheets [51], or with a combination of GelMA, PEGDA, PVA and alginate to generate textile-like hydrogel fibers with a dual crosslinking setup [52].

Here, the utilization of dissolvable MEW PCL patterns permits the generation of g-C_3N_4 hydrogels with controlled anisotropy to successfully induce neurite extension. Moreover, the versatility and precision of MEW provides a new platform for sacrificial patterning of hydrogels where any template could be designed for other desired tissue engineering organs, such as bone, muscle or cartilage.

4. Conclusions

In the present study, an anisotropic, electroactive, snapping g-C_3N_4/rGO based hydrogel system was successfully fabricated and adapted for NGCs. The incorporation of GO to the hydrogel network increased surface charges and intriguingly induced the snapping feature based on crosslinking gradient by the virtue of light penetration. All hydrogels were in the optimal mechanical stiffness range for peripheral nerve regeneration and were biocompatible with no cytotoxicity over PC12 cells, which were able to proliferate and differentiate in the hydrogels. Neural differentiation in the electroactive rGO (1 mg/mL and 3 mg/mL loading) hydrogels was found significantly higher compared to their counterparts. While a snapping NGC was obtained by a cross-sectional gradient of crosslinking of the tubular hydrogel, anisotropy was achieved by introducing sacrificial MEW microchannels in the hydrogels, where 10 μm was found to optimally guide enhanced neurite extension. The anisotropic, electroactive, self-snapping g-C_3N_4/rGO hydrogel NGC well supports neural cell growth and differentiation and thus holds great potential for repairing peripheral nerve injuries.

Credit author statement

JA, methodology, investigation, validation, formal analysis and writing- original draft; YS, methodology and Writing- original draft; FHS, ALF, SMS investigation and formal analysis; MD, conceptualization and resources; YF, Supervision; MC, conceptualization, methodology, resources, supervision, Writing-review &editing, funding acquisition.

Declaration of competing interest

The authors declare that they have no known competing financial interests or personal relationships that could have appeared to influence the work reported in this paper.

Data availability

Data will be made available on request.

Acknowledgement

We gratefully acknowledge Carlsberg Foundation (CF19-0300) and Sino Danish College for support of the research.

Appendix A. Supplementary data

Supplementary data to this article can be found online at https://doi.org/10.1016/j.mtbio.2022.100437.

References

[1] G. Blaauw, Review of "surgical disorders of the peripheral nerves" (2nd edition) by rolfe birch, J. Brachial Plexus Peripher. Nerve Inj. 7 (2012) 3, 3.
[2] R.M. Menorca, T.S. Fussell, J.C. Elfar, Nerve physiology: mechanisms of injury and recovery, Hand Clin. 29 (3) (2013) 317–330.
[3] G. Stoll, H.W. Muller, Nerve injury, axonal degeneration and neural regeneration: basic insights, Brain Pathol. 9 (2) (1999) 313–325.
[4] W.A. Lackington, A.J. Ryan, F.J. O'Brien, Advances in nerve guidance conduit-based therapeutics for peripheral nerve repair, ACS Biomater. Sci. Eng. 3 (7) (2017) 1221–1235.
[5] T. Gordon, N. Tyreman, M.A. Raji, The basis for diminished functional recovery after delayed peripheral nerve repair, J. Neurosci. 31 (14) (2011) 5325–5334.
[6] W.Z. Ray, S.E. Mackinnon, Management of nerve gaps: autografts, allografts, nerve transfers, and end-to-side neurorrhaphy, Exp. Neurol. 223 (1) (2010) 77–85.
[7] K.Y. Lee, D.J. Mooney, Hydrogels for tissue engineering, Chem. Rev. 101 (7) (2001) 1869–1880.
[8] M.W. Tibbitt, K.S. Anseth, Hydrogels as extracellular matrix mimics for 3D cell culture, Biotechnol. Bioeng. 103 (4) (2009) 655–663.
[9] L. Fan, et al., Directing induced pluripotent stem cell derived neural stem cell fate with a three-dimensional biomimetic hydrogel for spinal cord injury repair, ACS Appl. Mater. Interfaces 10 (21) (2018) 17742–17755.
[10] J.W. Nichol, et al., Cell-laden microengineered gelatin methacrylate hydrogels, Biomaterials 31 (21) (2010) 5536–5544.
[11] L.E. Bertassoni, et al., Hydrogel bioprinted microchannel networks for vascularization of tissue engineering constructs, Lab Chip 14 (13) (2014) 2202–2211.
[12] N.D. Leipzig, et al., Differentiation of neural stem cells in three-dimensional growth factor-immobilized chitosan hydrogel scaffolds, Biomaterials 32 (1) (2011) 57–64.
[13] K.H. Schmedlen, K.S. Masters, J.L. West, Photocrosslinkable polyvinyl alcohol hydrogels that can be modified with cell adhesion peptides for use in tissue engineering, Biomaterials 23 (22) (2002) 4325–4332.
[14] C.M. Valmikinathan, et al., Photocrosslinkable chitosan based hydrogels for neural tissue engineering, Soft Matter 8 (6) (2012) 1964–1976.
[15] Z. Tong, et al., Three-dimensional porous aerogel constructed by g-C3N4 and graphene oxide nanosheets with excellent visible-light photocatalytic performance, ACS Appl. Mater. Interfaces 7 (46) (2015) 25693–25701.
[16] B. Kumru, et al., Reinforced hydrogels via carbon nitride initiated polymerization, Macromolecules 50 (5) (2017) 1862–1869.
[17] C.A. DeForest, K.S. Anseth, Cytocompatible click-based hydrogels with dynamically tunable properties through orthogonal photoconjugation and photocleavage reactions, Nat. Chem. 3 (12) (2011) 925–931.
[18] J. Visser, et al., Reinforcement of hydrogels using three-dimensionally printed microfibres, Nat. Commun. 6 (2015).
[19] O. Bas, et al., Biofabricated soft network composites for cartilage tissue engineering, Biofabrication 9 (2) (2017).
[20] N. Dubey, et al., Highly tunable bioactive fiber-reinforced hydrogel for guided bone regeneration, Acta Biomater. 113 (2020) 164–176.
[21] Z. Zhang, et al., 3D anisotropic photocatalytic architectures as bioactive nerve guidance conduits for peripheral neural regeneration, Biomaterials 253 (2020), 120108.
[22] Y. Zhang, et al., 3D myotube guidance on hierarchically organized anisotropic and conductive fibers for skeletal muscle tissue engineering, Mater Sci Eng C Mater Biol Appl 116 (2020), 111070.
[23] M.L. Jørgensen, et al., A melt-electrowritten filter for capture and culture of circulating colon cancer cells, Materials Today Bio 6 (2020), 100052.
[24] L. Zhou, et al., Soft conducting polymer hydrogels cross-linked and doped by tannic acid for spinal cord injury repair, ACS Nano 12 (11) (2018) 10957–10967.
[25] W.B. Guo, et al., Construction of a 3D rGO-collagen hybrid scaffold for enhancement of the neural differentiation of mesenchymal stem cells, Nanoscale 8 (4) (2016) 1897–1904.
[26] Y. Zhou, et al., Highly stretchable, elastic, and ionic conductive hydrogel for artificial soft electronics, Adv. Funct. Mater. 29 (1) (2019), 1806220.
[27] M.B. Taskin, et al., *Poly(norepinephrine) as a functional bio-interface for neuronal differentiation on electrospun fibers*, Phys Chem Chem Phys 17 (14) (2015) 9446–9453.
[28] Z. Zhang, et al., Visible-light neural stimulation on graphitic-carbon nitride/graphene photocatalytic fibers, ACS Appl. Mater. Interfaces 9 (40) (2017) 34736–34743.
[29] G. Vunjak-Novakovic, et al., Dynamic cell seeding of polymer scaffolds for cartilage tissue engineering, Biotechnol. Prog. 14 (2) (1998) 193–202.
[30] G.A. Villalona, et al., Cell-seeding techniques in vascular tissue engineering, Tissue Eng. B Rev. 16 (3) (2010) 341–350.
[31] J.D. Roh, et al., Centrifugal seeding increases seeding efficiency and cellular distribution of bone marrow stromal cells in porous biodegradable scaffolds, Tissue Eng. 13 (11) (2007) 2743–2749.
[32] W.J. Ong, et al., Surface charge modification via protonation of graphitic carbon nitride (g-C3N4) for electrostatic self-assembly construction of 2D/2D reduced graphene oxide (rGO)/g-C3N4 nanostructures toward enhanced photocatalytic reduction of carbon dioxide to methane, Nano Energy 13 (2015) 757–770.
[33] X.F. Liu, et al., Functionalized carbon nanotube and graphene oxide embedded electrically conductive hydrogel synergistically stimulates nerve cell differentiation, ACS Appl. Mater. Interfaces 9 (17) (2017) 14677–14690.
[34] J. Park, et al., Electrically conductive hydrogel nerve guidance conduits for peripheral nerve regeneration, Adv. Funct. Mater. 30 (39) (2020).
[35] S.R. Shin, et al., Reduced graphene oxide-GelMA hybrid hydrogels as scaffolds for cardiac tissue engineering, Small 12 (27) (2016) 3677–3689.
[36] L.H. Klausen, T. Fuhs, M.D. Dong, Mapping surface charge density of lipid bilayers by quantitative surface conductivity microscopy, Nat. Commun. 7 (2016).
[37] T. Fuhs, et al., Direct measurement of surface charge distribution in phase separating supported lipid bilayers, Nanoscale 10 (9) (2018) 4538–4544.
[38] S.M. Sonderskov, et al., In situ surface charge density visualization of self-assembled DNA nanostructures after ion exchange, ChemPhysChem 21 (13) (2020) 1474–1482.
[39] N.Y. Sa, et al., Rectification of ion current in nanopipettes by external substrates, ACS Nano 7 (12) (2013) 11272–11282.
[40] G. Rosso, J. Guck, Mechanical changes of peripheral nerve tissue microenvironment and their structural basis during development, Apl Bioengineering 3 (3) (2019).
[41] S.A. Kruse, et al., Magnetic resonance elastography of the brain, Neuroimage 39 (1) (2008) 231–237.
[42] C. Hu, Y.R. Lin, H.C. Yang, Recent developments in graphitic carbon nitride based hydrogels as photocatalysts, ChemSusChem 12 (9) (2019) 1794–1806.
[43] V. Lovat, et al., Carbon nanotube substrates boost neuronal electrical signaling, Nano Lett. 5 (6) (2005) 1107–1110.
[44] Z. Zhang, et al., Electroactive scaffolds for neurogenesis and myogenesis: graphene-based nanomaterials, Small 14 (48) (2018) e1801983.
[45] W.X. Fan, et al., Dual-gradient enabled ultrafast biomimetic snapping of hydrogel materials, Sci. Adv. 5 (4) (2019).
[46] J. Wang, et al., Bioinspired multichannel nerve guidance conduit based on shape memory nanofibers for potential application in peripheral nerve repair, ACS Nano 14 (10) (2020) 12579–12595.
[47] E. Schnell, et al., Guidance of glial cell. migration and axonal growth on electrospun nanofibers of poly-epsilon-caprolactone and a collagen/poly-epsilon-caprolactone blend, Biomaterials 28 (19) (2007) 3012–3025.
[48] Y.T. Kim, et al., The role of aligned polymer fiber-based constructs in the bridging of long peripheral nerve gaps, Biomaterials 29 (21) (2008) 3117–3127.
[49] H.L. Qin, et al., Anisotropic and self-healing hydrogels with multi-responsive actuating capability, Nat. Commun. 10 (2019).
[50] M.J. Liu, et al., An anisotropic hydrogel with electrostatic repulsion between cofacially aligned nanosheets, Nature 517 (7532) (2015) 68–72.
[51] J.G. Torres-Rendon, et al., Cellulose nanofibril hydrogel tubes as sacrificial templates for freestanding tubular cell constructs, Biomacromolecules 17 (3) (2016) 905–913.
[52] A. Tamayol, et al., Hydrogel templates for rapid manufacturing of bioactive fibers and 3D constructs, Advanced Healthcare Materials 4 (14) (2015) 2146–2153.